Article:

Connolly, D., O'Malley, P. D., Akers, C. et al. (13 more authors) (2018) Direct measurement of resonance strengths in S 34 (α,γ) Ar 38 at astrophysically relevant energies using the DRAGON recoil separator. Physical Review C. 035801. pp. 1-12. ISSN 2469-9993

https://doi.org/10.1103/PhysRevC.97.035801

PHYSICAL REVIEW C **97**, 035801 (2018)

Direct measurement of resonance strengths in ^{34}S(α,γ)^{38}Ar at astrophysically relevant energies using the DRAGON recoil separator

D. Connolly,[1,*] P. D. O'Malley,[1,†] C. Akers,[2,3,‡] A. A. Chen,[4] G. Christian,[3,§] B. Davids,[3] L. Erikson,[5] J. Fallis,[3,‖] B. R. Fulton,[2] U. Greife,[1] U. Hager,[1] D. A. Hutcheon,[3] S. Ilyushkin,[1] A. M. Laird,[2] A. Mahl,[1] and C. Ruiz[3]
[1]*Department of Physics, Colorado School of Mines, Golden, Colorado 80401, USA*
[2]*Department of Physics, University of York, York, YO10 5DD, United Kingdom*
[3]*TRIUMF, Vancouver, British Columbia, V6T 2A3, Canada*
[4]*Department of Physics & Astronomy, McMaster University, Hamilton, Ontario, L8S 4K1, Canada*
[5]*Pacific Northwest National Laboratory, Richland, Washington 99352, USA*

(Received 31 January 2017; revised manuscript received 30 January 2018; published 7 March 2018)

Background: Nucleosynthesis of mid-mass elements is thought to occur under hot and explosive astrophysical conditions. Radiative α capture on ^{34}S has been shown to impact nucleosynthesis in several such conditions, including core and shell oxygen burning, explosive oxygen burning, and type Ia supernovae.
Purpose: Broad uncertainties exist in the literature for the strengths of three resonances within the astrophysically relevant energy range ($E_{\mathrm{CM}} = 1.94$–3.42 MeV at $T = 2.2$ GK). Further, there are several states in ^{38}Ar within this energy range which have not been previously measured. This work aimed to remeasure the resonance strengths of states for which broad uncertainty existed as well as to measure the resonance strengths and energies of previously unmeasured states.
Methods: Resonance strengths and energies of eight narrow resonances (five of which had not been previously studied) were measured in inverse kinematics with the DRAGON facility at TRIUMF by impinging an isotopically pure beam of ^{34}S ions on a windowless ^{4}He gas target. Prompt γ emissions of de-exciting ^{38}Ar recoils were detected in an array of bismuth germanate scintillators in coincidence with recoil nuclei, which were separated from unreacted beam ions by an electromagnetic mass separator and detected by a time-of-flight system and a multianode ionization chamber.
Results: The present measurements agree with previous results. Broad uncertainty in the resonance strength of the $E_{\mathrm{CM}} = 2709$ keV resonance persists. Resonance strengths and energies were determined for five low-energy resonances which had not been studied previously, and their strengths were determined to be significantly weaker than those of previously measured resonances.
Conclusions: The five previously unmeasured resonances were found not to contribute significantly to the total thermonuclear reaction rate. A median total thermonuclear reaction rate calculated using data from the present work along with existing literature values using the STARLIB rate calculator agrees with the NON-SMOKER statistical model calculation as well as the REACLIB and STARLIB library rates at explosive and nonexplosive oxygen-burning temperatures ($T = 3$–4 GK and $T = 1.5$–2.7 GK, respectively).

DOI: 10.1103/PhysRevC.97.035801

I. INTRODUCTION

Radiative α capture on ^{34}S (4.25% of $^{\mathrm{nat}}$S) producing ^{38}Ar (0.0629% of $^{\mathrm{nat}}$Ar) has been shown in network calculations to impact nucleosynthesis in several astrophysical environments and conditions, including (core and shell) oxygen burning [1], explosive oxygen burning (type II supernovae) [2–4], and type Ia supernovae [5]. Consequently, reaction rates involving ^{34}S and ^{38}Ar will influence final abundances of mid-mass elements ($28 \leqslant A \leqslant 62$) [2]. Experimentally, there exist broad uncertainties in the literature values for two strong resonances within the astrophysically relevant energy range for oxygen-burning temperatures that result in significant uncertainties in the stellar reaction rates at these temperatures. Additionally, there are several states in ^{38}Ar within the relevant energy range for which no ^{34}S + α resonance strength or energy measurements have been performed [6]. The astrophysical ^{34}S(α,γ)^{38}Ar reaction rate is expected to be dominated by resonant capture to natural parity states in ^{38}Ar lying above the α separation energy within the astrophysically relevant energy range, so accurate and precise calculation of the reaction rate depends strongly on experimental knowledge of the strength of these resonances.

---

[*] Present address: TRIUMF, Vancouver, BC, V6T 2A3, Canada; dconnolly@triumf.ca

[†] Present address: Department of Physics, University of Notre Dame, South Bend, IN, USA.

[‡] Present address: Rare Isotope Science Project, Institute for Basic Science, 70 Yuseong-daero 1689 gil, Yusung-gu, Daejeon 305-811, Korea.

[§] Present address: Department of Physics, Texas A & M University, College Station, TX, USA.

[‖] Present address: North Island College, Courtenay, BC, V9N 8N6, Canada.

TABLE I. Literature values for resonance strengths for the $^{34}\mathrm{S}(\alpha,\gamma)^{38}\mathrm{Ar}$ reaction. Values marked with an asterisk are those for which there exists a broad uncertainty in the published values. All CM resonance energies carry an uncertainty of ± 5 keV unless otherwise noted.

		Sinha *et al.* [9]		Erne and Van Der Leun [10]		Clarke *et al.* [11]	
$E_x^{(\mathrm{lit})}$ [MeV]	$J^{\pi}_{(\mathrm{lit})}$	E_{CM} [MeV]	$\omega\gamma$ [eV][a]	E_{CM} [MeV]	$\omega\gamma$ [eV][b]	E_{CM} [MeV]	$\omega\gamma$ [eV][a]
10.334	1^-	3.123(9)	1.6(4)			3.129	2.1
10.253	1^-	3.042(9)	2.6(6)			3.049	2.7
10.245	$(0^+ : 4^+)$	3.036(9)	<0.04				
10.217(9)	$(0^+ : 4^+)$	3.009(9)	0.04				
10.188	1^-	2.973(9)	4.9(1.2)			2.974	8.0
10.170	3^-	2.962	2.4(6)				
10.147	2^+	2.938(9)	0.3				
10.061	3^-	2.859	0.6				
10.047	(1^-)	2.839	0.04				
10.035	1^-	2.822	2.0(5)*	2.828	4.5(1.4)*		
9.993	1^-	2.781(9)	1.7(4)	2.788	3.0		
9.951	2^+	2.743	0.2				
9.917	1^-	2.703	2.62(56)*[c]	2.706	4.5(1.4)*		
9.894	2^+	2.686	0.6				
9.811	1^-	2.602	0.3	2.604	0.3		
9.797	3^-	2.589	0.3				
9.689	1^-	2.482	1.3(3)	2.480	1.5		
9.597	1^-	2.388	1.71(34)*[c]	2.389	4.0(1.2)*		

[a] Uncertainty ± 50% unless stated otherwise.
[b] Uncertainty ± 30% unless stated otherwise.
[c] Absolute resonance strength measurement.

^{34}S and subsequently ^{38}Ar are synthesized mainly through α capture on ^{30}Si, a product of the heavy-ion reactions ($^{16}\mathrm{O} + {}^{16}\mathrm{O}$) that occur during oxygen burning. Oxygen burning occurs in $M > 8\,M_{\odot}$ stars near the end of their evolution during the blue supergiant phase. Core oxygen burning typically occurs at temperatures of $T = 1.5$–2.7 GK, whereas shell oxygen burning occurs at somewhat higher temperatures [1]. At a nominal temperature of $T = 2.2$ GK (typical for core oxygen burning), the astrophysically relevant energy range for radiative α capture on ^{34}S spans 1.94–3.42 MeV in the center of momentum (CM) frame [7]. The primary ashes of oxygen burning are ^{28}Si and ^{32,34}S [8]. Network calculations [1,8] predict that the most abundant nuclides at the end of oxygen burning are $^{28}\mathrm{Si}(X_f = 0.54)$, $^{32}\mathrm{S}(X_f = 0.28)$, $^{38}\mathrm{Ar}$ ($X_f = 0.084$), ^{34}S ($X_f = 0.044$), ^{36}Ar ($X_f = 0.027$), and ^{40}Ca ($X_f = 0.021$). However, the mass fraction of ^{34}S at the end of oxygen burning can be as high as 0.16 in more massive ($\sim 25\,M_{\odot}$) stars [8].

Explosive oxygen burning occurs in core collapse (type II) supernovae typically at temperatures of $T = 3$–4 GK. Synthesis up to the iron peak along the main line of stability ($A = 2Z$) is bottlenecked at Sc and Ti, which quickly photodisintegrate at these temperatures because these nuclides are weakly bound relative to the magic proton number isotopes of Ca ($Z = 20$) [4]. On the other hand, nucleosynthesis *can* proceed along the neutron-rich path $A = 2(Z + 1)$, where nuclides are more tightly bound than at the main line of stability [4]. Therefore $^{34}\mathrm{S}(\alpha,\gamma)^{38}\mathrm{Ar}$ provides an important channel for nucleosynthesis up to the iron peak.

A recent sensitivity study also showed that radiative α capture on ^{34}S could impact nucleosynthesis in type Ia supernovae [5]. The authors of Ref. [5] varied the reaction rate for specific reactions (among a reaction network) by factors of 0.1 and 10 and compared the mass ejecta of nuclides to a reference model (a one-dimensional delayed detonation model DDTc [12] with a Chandrasekhar mass O-Ne-Mg white dwarf progenitor and a deflagration to detonation transition density of $2.2 \times 10^7\,\mathrm{g\,cm^{-3}}$). In the study, $0.029 M_{\odot}$ (or about 2% of the total mass) were processed thorough the $^{34}\mathrm{S}(\alpha,\gamma)^{38}\mathrm{Ar}$ channel in the reference model, and increasing (decreasing) the enhancement factor by an order of magnitude resulted in the yields of ^{38}Ar and ^{39}K being enhanced (reduced) by 12–100%.

II. PREVIOUS MEASUREMENTS

When comparing the published results from past $^{34}\mathrm{S}(\alpha,\gamma)^{38}\mathrm{Ar}$ experiments [3,9–11,13,14], one observes a discrepancy of about a factor of 2 in the literature for the nominal value of the strength of three resonances in $^{34}\mathrm{S}(\alpha,\gamma)^{38}\mathrm{Ar}$ within the astrophysically relevant energy range for oxygen-burning temperatures (see Table I). The resulting uncertainty in these resonance strengths leads to a significant uncertainty in the narrow resonance reaction rate in this energy range. Further, the $^{34}\mathrm{S}(\alpha,\gamma)^{38}\mathrm{Ar}$ astrophysical reaction rate is expected to be dominated by the resonant capture to natural parity states above the α separation energy in ^{38}Ar lying within the astrophysically relevant energy range (1.94–3.42 MeV at $T = 2.2$ GK). Additionally, it is clear from transfer reactions [6] and heavy-ion fusion evaporation reactions [15] that there exist states in ^{38}Ar within the relevant energy range for which radiative α-capture resonance strengths have not been measured (see Fig. 1).

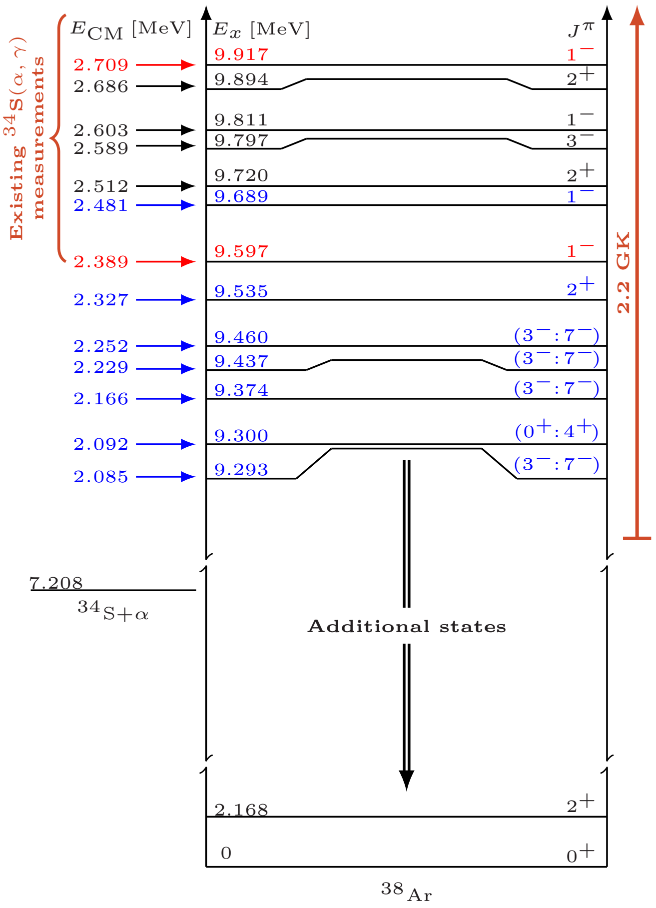

FIG. 1. Partial level diagram of ^{38}Ar. States in blue were measured in this work. The two states in red (also measured in this work) are those for which there exists broad uncertainty in the literature values for the resonance strengths. Excitation energies are those reported in Ref. [16]. The astrophysically relevant energy range for oxygen burning (calculated from Ref. [7]) is illustrated on the right.

The previous ^{34}S(α,γ)^{38}Ar experiments were conducted using solid composite targets. The systematic uncertainties of such measurements typically include problems due to unknown stoichiometry or possible changes under beam bombardment as well as lack of information on stopping power and energy straggling throughout the target. As a response, often one or two stronger resonances are selected as standards for which an absolute yield measurement is performed (and evaluated) while other resonances are then measured relative to them under the assumption of constant stoichiometry and a model for the energy dependence of the stopping power (typically the SRIM code [17,18]).

There are several states above the α separation energy (Q = 7.208 MeV [19]) that are known from previous ^{34}S(α,γ)^{38}Ar measurements [9,10,20] (see Fig. 1). The states at E_x = 9917(5) keV and E_x = 9597(5) keV are those for which there exists broad uncertainty in the literature for the measured resonance strength, and the minimum energy to which prior ^{34}S(α,γ) measurements probed is E_x = 9597 keV. A J^π = 2^+ state at E_x = 9720(20) keV has been observed in the ^{36}Ar(t,p)^{38}Ar transfer reaction [21], but remains unmeasured in the (α,γ) channel as it is not expected to contribute significantly to the reaction rate. Other states in the energy region of interest for this experiment (for example, a 1^+ state at E_x = 9431 keV known from ^{38}Ar(e,e') [22] and a state of tentative J^π = (4^- to 8^-) at E_x = 9829(2) keV known from fusion evaporation [15]), have been omitted from Fig. 1 for clarity, because population of these states is expected to be strongly suppressed, owing to their unnatural parity. Additionally, population of high-angular-momentum states is unlikely due to the considerable Coulomb + angular momentum potential barrier height and low-α penetration factor at the energies considered. A doublet of states exists near E_x = 9535 keV: Flynn *et al.* [21] observed a J^π = 2^+ state at E_x = 9530 ± 20 keV in the ^{36}Ar(t,p)^{38}Ar transfer reaction and a state of tentative J^π = (8^+) at E_x = 9537.2(4) keV is known from ^{35}Cl($\alpha,p\gamma$)^{38}Ar. The uncertainty of 3 keV quoted in Ref. [16] for the E_x = 9535 keV state appears to have been taken from Glatz *et al.* [15], who observed a state at E_x = 9535 ± 3 keV in ^{35}Cl($\alpha,p\gamma$)^{38}Ar. Glatz *et al.* [15] did not assign a spin parity to this state [although they did observe electromagnetic transitions to states of J^π = 8^+ and (8^+)] but Kern *et al.* [23] later assigned a tentative J^π = (7^+). Therefore, the energy uncertainty of ±3 keV attributed to the J^π = 2^+ state at E_x = 9535 keV likely belongs to the high-spin state of J^π = (8^+) at E_x = 9537.2(4) [16]. Finally, there exist several low-spin states above the α threshold in ^{38}Ar at energies lower than those measured in this work (e.g., two J^π = 1^- states at 7.376 and 7.857 MeV and two J^π = 2^+ states at 8.668 and 8.391 MeV), but due to the rapidly decreasing Coulomb penetrability at low α energies, these states are inaccessible to direct resonance strength measurement. Furthermore, these states are not expected to contribute to the astrophysical reaction rate at explosive- and nonexplosive oxygen-burning temperatures (T = 3–4 GK and T = 1.5–2.7 GK, respectively).

III. EXPERIMENTAL

The experiment was conducted in inverse kinematics at the Detector of Recoils and Gammas of Nuclear Reactions (DRAGON), which is located in the Isotope Separator and ACcelerator-I (ISAC-I) experimental hall at TRIUMF. An isotopically pure beam of ^{34}S ions was generated by the Supernanogan [24] electron cyclotron resonance (ECR) plasma source using a gas supply of SF$_6$ enriched in ^{34}S. The beam was accelerated through the ISAC-I Radio-Frequency Quadrupole (RFQ) and the Drift-Tube Linac (DTL) to energies between 20.23 and 25.75 MeV ($E_{\rm CM}$ = 2.133–2.714 MeV) and delivered to DRAGON's windowless gas target at an average intensity of 6.79×10^9 s^{-1} in the 7+ charge state. The beam energy spread was $\Delta E/E \leqslant 0.4\%$ (FWHM) [25] for all energies.

The DRAGON recoil mass separator [26] (see Fig. 2) consists of three main components: (1) a windowless gas target and γ-detector array, (2) an electromagnetic mass separator (EMS) consisting of magnetic dipoles, quadrupoles, and sextupoles, two electrostatic dipoles as well as slits at the focal planes of the various separation stages for recoil separation and beam

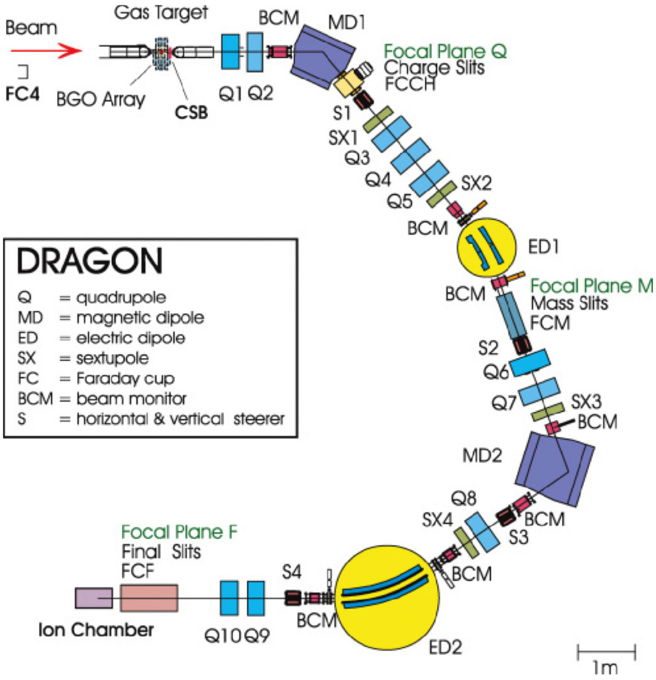

FIG. 2. Schematic of the DRAGON recoil mass separator.

suppression and (3) a configurable series of heavy ion detectors [28] situated at the final focal plane of the separator for recoil particle identification. DRAGON's γ detector array consists of 30 bismuth germanate (BGO) scintillators in a close-packed geometry covering 92% of the solid angle surrounding the gas target. The heavy ion detector configuration used in the present work was a transmission time of flight (TOF) system, consisting of dual microchannel plate (MCP) detectors, in series with a multi-anode ionization chamber (IC) which measured the energy loss and total kinetic energy of heavy ions transmitted to DRAGON's focal plane. A state-of-the-art, time-stamp-based data acquisition (DAQ) system is used to process all of the data collected by DRAGON's various detectors and diagnostics [29]. In contrast to experiments using solid composite targets, the DRAGON approach using a heavy-ion beam impinging on a pure helium windowless gas target in inverse kinematics avoids all stoichiometry issues and is also able to measure the stopping power (necessary for resonance strength extraction) precisely at each experimental energy. The helium gas target has an effective length of 12.3 cm [26] and was operated at pressures ranging from 7.08 to 9.13 Torr. This resulted in target thicknesses ranging from 55 to 75 keV in the CM system (illustrated in Fig. 9), all of which are significantly larger than the expected individual resonance widths. The present work measured the strengths and energies of eight resonances in $^{34}\mathrm{S}(\alpha,\gamma)^{38}\mathrm{Ar}$. All of these resonances fall within the astrophysically relevant energy range for oxygen-burning temperatures (see Fig. 1) and, consequently, some of these resonances have a significant impact on the astrophysical reaction rate of $^{34}\mathrm{S}(\alpha,\gamma)^{38}\mathrm{Ar}$ at explosive and nonexplosive oxygen-burning temperatures. For further details of the DRAGON EMS, see references [26–30] and the references therein.

IV. DATA ANALYSIS

Nine yield measurements were made at eight beam energies corresponding to the aforementioned states in $^{38}\mathrm{Ar}$. Incident $^{34}\mathrm{S}$ beam energies were chosen to place the position of resonant captures (as calculated from literature value of resonance energy) in the center of the target. Over the energy range for which no previous measurements existed, beam energies were chosen to provide an overlap of energy ranges covered.

A. Thick target yield and resonance strength

Laboratory experiments of radiative capture reactions measure the *yield* of the reaction, which is defined as

$$Y = \frac{N_{\text{rxns.}}}{N_{\text{b}}}, \tag{1}$$

where N_b is the total number of beam particles incident on the target volume and $N_{\text{rxns.}}$ is the number of radiative capture reactions of interest that occurred in the experiment. DRAGON measures the number of *recoils* from reactions occurring within the target volume (via its heavy-ion detectors) and then one infers the number of reactions based on the systematics of the experimental setup. Thus DRAGON's yield is given by

$$Y = \frac{N_{\text{rec}}}{\eta_{\text{DRA}} N_{\text{b}}} \tag{2}$$

where η_{DRA} is DRAGON's total recoil detection efficiency. The recoil detection efficiency can vary from experiment to experiment according to the methods used to identify recoils. For the purposes of this work, DRAGON's recoil detection efficiency for singles events[1] in DRAGON's heavy-ion detectors is given by

$$\eta_{\text{DRA}}^{\text{sing}} = f_q \, \tau_{\text{sep}} \, \tau_{\text{MCP}} \, \eta_{\text{MCP}} \, \eta_{\text{IC}} \, \lambda_{\text{tail}}, \tag{3}$$

where f_q is the charge state fraction of the selected recoil charge state, τ_{sep} is the separator transmission (taken as $0.999^{+0.001}_{-0.002}$ for the purposes of this work [31]), τ_{MCP} is the geometric transmission of the MCP, η_{MCP} is the MCP detection efficiency, η_{IC} is the IC detection efficiency, and λ_{tail} is the live time fraction of the focal plane DAQ.

When (as is the case for all resonances measured in this work) the resonance width is small compared to the energy thickness of the target (which was between 55 and 75 keV in the CM system for all yield measurements), the reaction yield becomes the thick target yield (i.e., $Y \rightarrow Y_\infty$). The thick target yield for a narrow Breit-Wigner resonance is related to the resonance strength by [32]

$$\omega\gamma = \frac{2Y_\infty}{\lambda_r^2} \frac{m_p}{m_p + m_t} \epsilon_{\text{lab}} \tag{4}$$

where $\omega\gamma$ is the resonance strength, m_p and m_t are the masses of the projectile and target nuclei (respectively), ϵ_{lab} is the laboratory frame stopping power, and λ_r is the de Broglie wavelength of the resonance (in the CM frame). In addition to

---

[1] Events detected in the end detector without requiring a coincident event in DRAGON's BGO γ array.

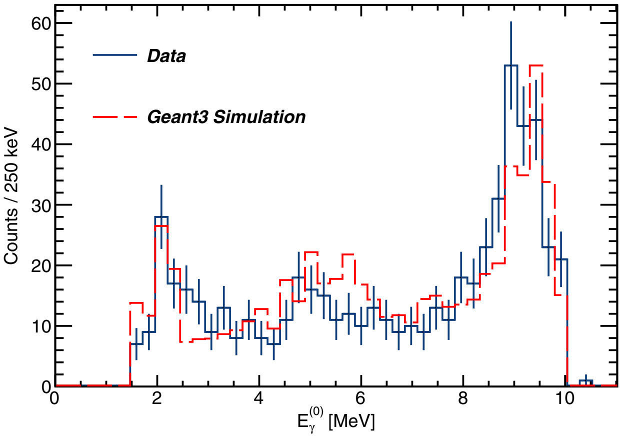

FIG. 3. BGO γ-ray array energy spectrum of highest energy γ per event for the 2389-keV resonance (blue) compared to GEANT-3 simulation (red).

the thick target yield, the extraction of the resonance strength also requires knowledge of the laboratory frame stopping power, which was measured directly in this experiment.

B. Particle identification in coincidence

When (as is the case for this work) an isotopically pure ion beam can be delivered to the DRAGON experiment, in principle, the simplest and most background-free method of determining the reaction yield of an (α,γ) reaction is to measure the coincidences between the detection of a γ-ray in the BGO array and a heavy-ion recoil at the focal plane of the separator. However, such an analysis requires [in addition to the efficiency factors listed in Eq. 3] simulation of the BGO γ-ray array efficiency for (sometimes unknown) de-excitation γ energy distributions from the population of a specific state in the product nucleus. In this (usually iterative) process using a GEANT-3 simulation of DRAGON's BGO γ-ray array [27], the measured coincident γ-ray spectra in the array are fitted with the expected response to a distribution informed by the compiled knowledge of the nucleus in question. Branching ratios are varied until a good fit is achieved. An example of the result of such a procedure is shown in Fig. 3 where the highest energy γ deposit per event is displayed for the complete BGO array compared to the outcome of the GEANT informed fit.

Naturally, this process introduces an additional source of uncertainty into the extraction of the reaction yield, making it preferable, if possible, to use only the evaluation of heavy-ion recoil events in DRAGON's end detectors in the analysis. However, the information from the coincidence analysis in all cases provides important information on the identification of the reaction recoil events in the focal plane detectors as well as a good check on the validity of compiled decay schemes for the excited states populated.

C. Particle identification in singles

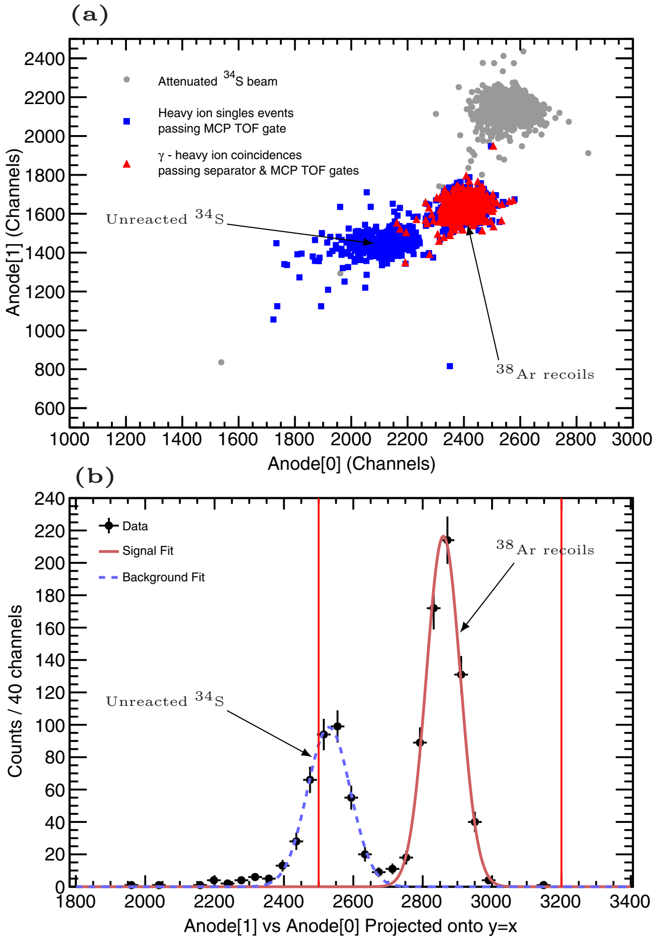

FIG. 4. (a) Overlay of ionizaiton chamber spectra displaying the response of the first two anodes to attenuated ^{34}S beam (grey circles), singles IC events (blue squares) and $\gamma-$ heavy ion coincidences subjected to gates on the separator TOF and MCP TOF (red triangles - see text for detailed explanation). (b) Projection of panel (a) onto the anode[0] = anode[1] axis allowing for a double Gaussian fit to extract recoil statistics. Vertical lines indicate the selected signal region.

In cases where the beam suppression of the electromagnetic separator alone is sufficient to provide clean identification of recoil events in the focal plane detectors, the reaction yield can be extracted from an analysis of singles events incident on the IC. Here, particle identification is achieved by plotting the ion energy loss in anode segments against one another and observing the largest separation between beam and recoil ion type through their differences in stopping power in the detection medium.

Figure 4(a) shows an overlay of a $dE-dE$ spectra displaying the response of the first two anodes of the IC (anode[0] and anode[1]) to attenuated ^{34}S beam (gray circles), singles[2] IC events passing a gate on the MCP time of flight (the time difference between signals in two MCP detectors that straddle DRAGON's focal plane) when the DRAGON separator was tuned to the A/q of ^{38}Ar recoils (blue circles) and coincident γ–heavy-ion events passing a gate on the separator TOF (time

---

[2] Heavy-ion "singles" events are all events detected in the DRAGON end detector (the IC in this case), regardless of whether a coincident γ event was detected in the BGO array.

difference between a coincident BGO γ hit and the heavy-ion MCP TOF start; red triangles partially obscuring the singles recoil hit pattern) for all data collected at an incident beam energy of 23.036 MeV (i.e., the yield measurement of the 2389-keV resonance). The γ–heavy-ion coincidence events clearly identify the locus of events centered near anode[0] channel 2400 and anode[1] channel 1650 as the ^{38}Ar recoil signal. The locus of events (near anode[0] channel 2100 and anode[1] channel 1450) are unreacted ^{34}S ions transmitted to DRAGON's focal plane detector. Unreacted ^{34}S events do not populate in the same region as the events recorded during an attenuated beam run (gray circles) because DRAGON's exceptional beam suppression for (α,γ) reactions ensures that only those unreacted beam ions that have undergone at least one charge and/or energy changing reaction are transmitted to the focal plane. The singles $dE - dE$ plot projection onto the anode[0] = anode[1] axis is displayed in Fig. 4(b). The resulting 1-D pulse height spectra were fit with a double Gaussian. In order to estimate the signal (reaction recoils) to background (unreacted beam) ratio, a signal region was defined to encompass all events passing the separator TOF gate [see Fig. 4(b)]. The background was estimated by integrating the background distribution over the limits of the signal region, and the recoil yield was estimated by subtracting the background estimate from the total number of events in the signal region using the methods outlined in Ref. [33], assuming Gaussian detection efficiency and background models at the 68% confidence level.

D. Beam normalization

In order to determine the number of beam nuclei incident on DRAGON's gas target ($N_{\rm b}$), the beam was continuously monitored during data collection by detecting elastically scattered ^{4}He nuclei with a pair of ion-implanted silicon (IIS) charged-particle detectors mounted inside the gas target volume. The data were normalized to regular Faraday cup (FC) readings of the beam current via a FC (FC4, see Fig. 2) approximately 2 m upstream of the target. FC readings were taken at the beginning and end of each hour-long run. The relationship between beam current (FC4 current readings) and number of elastically scattered target nuclei leads to a normalization coefficient R, which can be calculated for a given run as

$$R = \frac{I}{q\,e}\frac{\Delta t\,P}{N_\alpha}\eta_{\rm tgt.}, \tag{5}$$

where N_α is the number of ^{4}He nuclei scattered into the IIS detector within a time window Δt, I is the current reading on FC4, e is the elementary charge, q is the beam charge state (7+), P is the target pressure (Torr), and $\eta_{\rm tgt.}$ is the beam transmission through an empty target. An average normalization coefficient over all runs (for given yield measurement at energy E) can then be computed by fitting a constant $\overline{R}$ to the normalization data (see Fig. 5), and the total number of beam particles ($N_{\rm b}$) incident on the gas target volume can then be calculated as

$$N_{\rm b} = \frac{\overline{R}\,N_\alpha}{P}, \tag{6}$$

where N_α is the total number of α detected by the IIS detectors during the yield measurement.

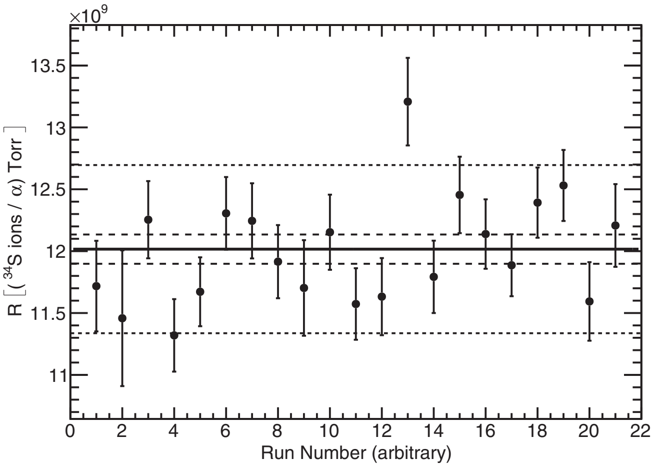

FIG. 5. Beam normalization coefficients R for all runs during the yield measurement of the $E_{\rm CM} = 2166$ keV resonance. The solid horizontal line is the value of $\overline{R}$ obtained from a χ^2 fit to the data. Dashed horizontal lines are the statistical uncertainty in $\overline{R}$, and dotted horizontal lines are the total (statistical and systematic added in quadrature) uncertainty in $\overline{R}$.

E. ^{34}S stopping power in ^{4}He

Often, laboratory measurements of nuclear reaction yields do not directly measure the stopping power (due to a variety of factors) [1,34], so one must rely on semiempirical model calculations of the stopping power in order to calculate resonance strengths. Typically, when experimental values exist, the model calculations describe the real stopping powers well. However, when no experimental data exists, or when extrapolation (interpolation) to (between) other energy regimes is necessary, discrepancies on the order of 10% have been observed [34]. DRAGON is able to make direct stopping power measurements by varying the target pressure and subsequently measuring the (changed) magnetic field strength required to center the beam in the energy-dispersed focal plane.

Stopping power measurements were performed with the ^{34}S ion beam at all beam energies for which yield data were taken. The stopping power was then used in Eq. 4 to calculate the resonance strength. Figure 6 compares the stopping power measurements of the present work to that of the Stopping and Range of Ions in Matter (SRIM) model calculation [17,18]. From Fig. 6, it is apparent that the experimentally measured stopping power differs from the model calculation by ∼10–15%.

F. Ar charge state distributions

DRAGON transports only a fraction of the experimental recoil yield to the focal plane due to the selection of a single charge. In order to calculate the total number of recoils produced, experiments conducted at DRAGON typically include measurements of the charge state distribution (CSD) of a beam of a stable and abundant isotope of the recoil species. For the present work, a stable beam of ^{40}Ar was used. However, DRAGON's first magnetic dipole is limited in its bending power [30] and, consequently, the CSD of ^{40}Ar in ^{4}He was

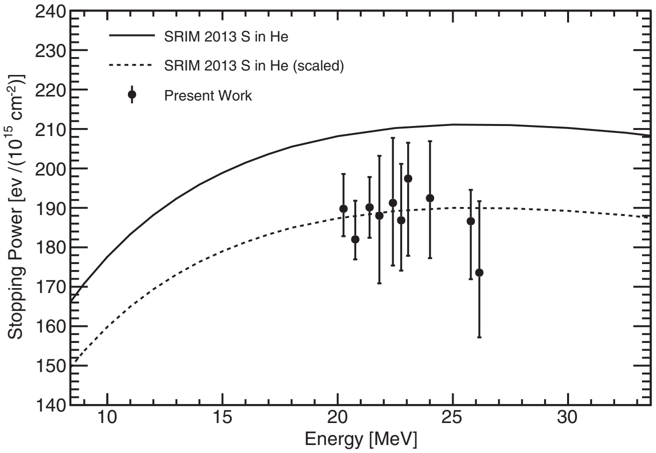

FIG. 6. Comparison of stopping power of ^{34}S in ^{4}He to SRIM 2013 calculation. The dashed line represents the SRIM 2013 calculation scaled by a factor of 0.9.

reliably measured at only one beam energy in the present work. Therefore, only incomplete distributions (which are difficult to normalize) could be compared to semiempirical formulas [35,36] based on similar measurements. Figure 7 shows a comparison of the approximately normalized data from this work with the semiempirical formulas of Refs. [35,36]. In the present work, values resulting from the application of Ref. [35] (using the distribution width parameters[3] from Liu *et al.* [36]) were used in yield calculations.

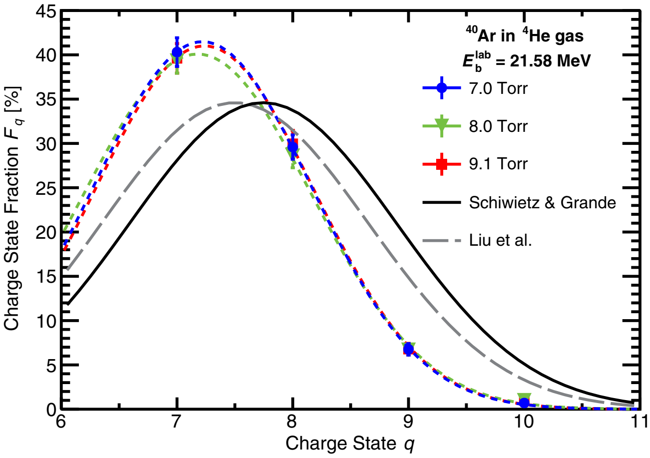

FIG. 7. CSD measurements of ^{40}Ar passing through ^{4}He gas at a laboratory-frame bombarding energy of $E_b^{\rm lab} = 21.58$ MeV. The black and dashed gray curves are the average equilibrium CSDs predicted by the semi-empirical formulas of Refs. [35,36], respectively.

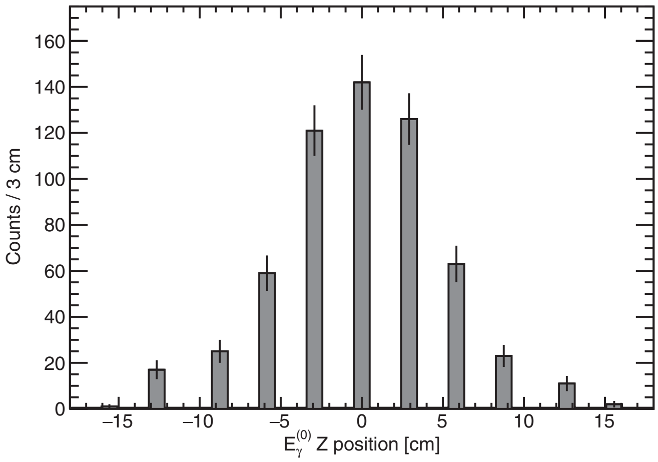

FIG. 8. BGO z-position spectrum of the highest energy γ-ray per event for (coincident) events passing all recoil cuts for the 2388-keV resonance measurement.

G. Resonance energy determination

The measured resonance energies were calculated from the geometric mean of the distribution of the z position (position along the beam axis) of the highest energy γ per event detected in the BGO array for events passing all recoil cuts (see Fig. 8). Combining this information with the energy loss across the target and stopping power, one may calculate the resonance energy using Eqs. (3)–(5) from Ref. [37]. Note that the calculation of resonance energies in this work exclude the geometric correction (i.e., the systematic offset of 0.57 cm due to the "less efficient two upstream BGO counters") from Eq. (3) of Ref. [37] because the two less efficient upstream detectors were in their normal position for stable beam measurements (i.e., the BGO array was symmetric with respect to the z axis). Where possible (i.e., when the outgoing beam energy from the gas target was approximately equal to or overlapped with the next measurement's incoming beam energy), the stopping power parameter $\mathcal{R}$ was calculated using measured values for E, S, ΔE, and ΔS. Otherwise, it was calculated using interpolated values from the SRIM calculation [17,18] scaled by a factor of 0.9.

H. Uncertainties

The dominant source of statistical uncertainty in the present measurements originates from the counting statistics of ^{38}Ar recoils in DRAGON's heavy-ion detectors (using the analysis methods outlined in Ref. [33] and assuming Gaussian background and detection efficiency models at the 68% confidence level). There is also a significant contribution from the statistical uncertainty in the measured stopping power. For most of the resonance measurements, the dominant source of systematic uncertainty originated from the (calculated) charge state fraction, which ranged from 0.4% for the 2709-keV resonance to 15.4% for the 2327-keV resonance. The large uncertainty in the charge state fraction (CSF) arises from the absolute systematic uncertainty in the calculated average equilibrium charge state in the semiempirical formula

---

[3] Schiwietz and Grande do not give width parameters for their formula in the case of gas strippers, so the present work uses the width parameters given by Liu *et al.* [36].

TABLE II. Relative systematic uncertainties used to calculate the resonance strength of the 2389-keV resonance (1σ).

Source	Uncertainty
Charge state fraction, η_{CSF}	14.65%
Beam normalization, R	5.70%
Stopping power	2.37%
MCP transmission, $\eta_{\mathrm{MCP}}^{\mathrm{Trans}}$	1.00%
Beam energy [25,37]	0.24%
Separator transmission, η_{Sep}	0.20%
MD1 constant [37]	0.15%
Total systematic uncertainty	15.94%

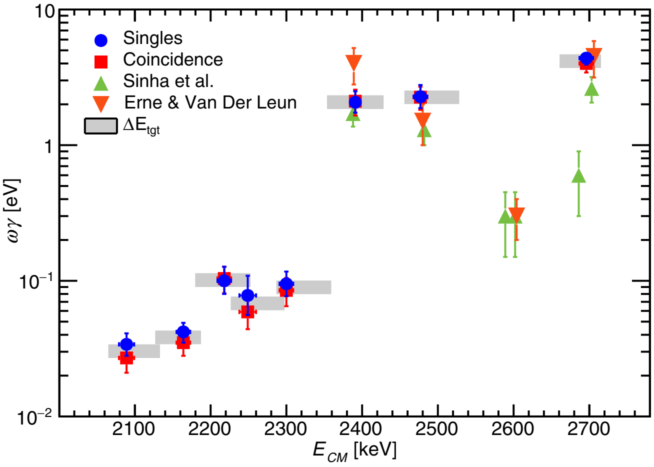

FIG. 9. Resonance strength vs CM energy from the present work (singles and coincidence) compared with literature values [9,10]. Gray bars indicate the energy thickness (55–75 keV in the CM system) of the gas target during the yield measurement. Statistical and systematic uncertainties are displayed combined in quadrature.

from Ref. [35]. For measurements in which the systematic uncertainty in the CSF was low, the dominant source of systematic uncertainty originated from beam normalization. Other sources of experimental uncertainty are shown for the analysis of the 2389-keV resonance in Table II as an example. These systematic uncertainties are combined in quadrature with statistical uncertainties for each measurement.

V. RESULTS AND DISCUSSION

This experiment provided a remeasurement of several resonances in the $^{34}\mathrm{S}(\alpha,\gamma)^{38}\mathrm{Ar}$ reaction and extracted new resonance strengths for several previously unmeasured states. The resonance energies measured in this work agree with existing data at the 2σ level. As noted in Sec. II, a $J^\pi = 2^+$ state at $E_x = 9535(20)$ keV was observed in ^{38}Ar via two-neutron transfer on ^{36}Ar [21]. The canonical [16] uncertainty of ±3 keV assigned to this excitation energy is likely misattributed to this state, and more appropriately belongs to the high-spin state of tentative $J^\pi = (8^+)$ at 9537.2(4) keV observed in $^{35}\mathrm{Cl}(\alpha,p\gamma)^{38}\mathrm{Ar}$ [15]. Because of the large uncertainty in the canonical value for this state, the excitation energy of $E_x = 9508(9)$ keV measured in this work agrees with the value of $E_x = 9535(20)$ keV measured by Flynn *et al.* [21].

The data collected in this work agree with both the Sinha *et al.* [9] and the Erne and Van Der Leun [10] data. However, because there were two resonances in the target (see Fig. 9) for the yield measurement of the $E_{\mathrm{CM}} = 2709$ keV resonance, the broad uncertainty in its resonance strength persists. Additionally, yield measurements were performed for five low-energy intervals which had not been covered previously and resonance strengths and energies were extracted from these yield measurements. The strengths of the measured resonances (where the highest and lowest energy intervals each cover two resonant states), analyzed by the aforementioned singles and coincidence methods are displayed together with the previous measurements in Table III, as well as in Fig. 9. It can be seen that these five resonances are significantly weaker

TABLE III. Resonance strengths and energies measured in this work compared to literature values.

$E_x^{(\mathrm{lit})}$ [keV]	$J^\pi_{(\mathrm{lit})}$	$E_{\mathrm{CM}}^{(\mathrm{lit})}$ [keV]	$E_{\mathrm{CM}}^{(\mathrm{meas})}$ [keV]	$\omega\gamma_{\mathrm{sing}}$ [eV]	$\omega\gamma_{\mathrm{coinc}}$ [eV]	$\omega\gamma$ [eV] [9]	$\omega\gamma$ [eV] [10]
9917(5)	1^-	2709(5)	2696(9)[a]	4.38(0.46)[b]	4.01(57)[b]	2.62(56)[c]	4.5(1.4)[d]
9689(5)	1^-	2481(5)	2477(9)	$2.28^{+0.50}_{-0.40}$	2.26(44)	1.3(3)	1.5(5)
9597(5)	1^-	2389(5)	2391(8)	$2.07^{+0.43}_{-0.34}$	2.11(46)	1.71(34)	4.0(1.2)
9535(20)	2^+	2327(20)[e]	2300(9)	$0.095^{+0.022}_{-0.018}$	0.085(20)		
9460(2)	$(3^- : 7^-)$	2252(2)	2249(11)	$0.078^{+0.031}_{-0.022}$	0.059(15)		
9437(2)	$(3^- : 7^-)$	2229(2)	2218(9)	$0.100^{+0.027}_{-0.020}$	0.104(23)		
9374(2)	$(3^- : 7^-)$	2166(2)	2164(9)	0.042(0.007)	0.035(7)		
9300(4)/9293(2)	$(0^+ : 4^+)/(3^- : 7^-)$	2092(4)/2085(2)	2089(10)[f]	0.045(0.007)[g]	0.027(6)[g]		

[a] Calculated from γ_0 Z-distribution weighted mean of 2706- and 2686-keV resonances.
[b] Combined $\omega\gamma$ of 2706- and 2686-keV resonances.
[c] Resonance strength of 2706-keV resonance.
[d] Likely combined $\omega\gamma$ of 2706- and 2686-keV resonances.
[e] See discussion in Sec. II regarding energy uncertainty of this state.
[f] Calculated from γ_0 Z-distribution weighted mean of 2092- and 2085-keV resonances.
[g] Combined $\omega\gamma$ of 2092- and 2085-keV resonances.

than the resonances at 2709, 2481, and 2389 keV and therefore, although lower in energy, do not contribute significantly to the total thermonuclear reaction rate as is illustrated in Fig. 11. Because of the good agreement resonance strengths obtained by singles and coincidence analyses, only data from the singles analysis is considered in the following discussion.

Because of the overlap of the energies covered by the gas target during the yield measurements $E_{\rm CM} = 2089$–2300 keV, it is possible that neighboring resonances contributed to the measured yield of these resonances. For example, during the yield measurement at $E_{\rm CM} = 2252$ keV, the energy thickness of the gas target overlapped with the previous yield measurement of the $E_{\rm CM} = 2300$ keV resonance (and similarly for the yield measurement of the $E_{\rm CM} = 2218$ keV resonance; see Fig. 9). However, for these yield measurements, the intruding resonance would have been placed at the upstream edge of the gas target, meaning only the tail of the intruding resonance would contribute to the measured yield. Therefore, any contribution from neighboring resonances is deemed to be negligible.

In order to compare the total thermonuclear reaction rate from experiments to theoretical Hauser-Feshbach calculations and existing library rates, a median total thermonuclear reaction rate was calculated using the STARLIB [38] rate calculator. The STARLIB rate calculation method assumes appropriate probability density functions (pdf) for each physical quantity used in the rate calculation which are then randomly sampled to calculate a median rate and requisite cumulative distribution function (cdf) [38,39]. Estimation of the reaction rate uncertainty ("high" and "low" rates) are based on the $1-\sigma$ quantiles of the reaction rate cdf. Thus uncertainties in the physical data are propagated to the reaction rate in a statistically rigorous and meaningful way. As input for the STARLIB calculation, the data from the eight resonance strengths measured in this work was combined with the tabulated data [9–11,13,14] of other known states up to $E_{\rm CM} = 4.234$ MeV ($E_x = 11.442$ MeV). Resonance strengths and energies were adopted from the reference noted in Table IV (for cases in which only one measurement exists); otherwise the weighted averages of resonance strengths and energies (and

TABLE IV. Resonance energies and strengths used to calculate the total reaction rate shown in Fig. 11 using the STARLIB rate calculator [38] (see text for details).

$E_{\rm CM}$[keV]	$\omega\gamma$[eV]
2089.4(10.0)[a]	0.034(7)
2164.4(9.0)[a]	0.042(7)
2217.6(10.0)[a]	0.100(27)
2248.5(11.0)[a]	0.078(31)
2299.7(10.0)[a]	0.095(22)
2388.4(3.0)[b]	1.95(26)
2480.3(3.0)[b]	1.54(22)
2589.0(4.5)[b]	0.30(15)
2603.2(3.2)[b]	0.30(8)
2685.5(4.5)[c]	0.60(30)
2704.0(3.0)[b]	3.72(34)
2742.8(4.5)[c]	0.20(10)
2786.3(4.0)[b]	2.31(62)
2825.1(3.2)[b]	2.89(80)
2838.5(4.5)[c]	0.04(02)
2859.1(4.5)[c]	0.60(02)
2937.8(8.9)[c]	0.30(15)
2962.0(4.5)[c]	2.4(6)
2973.5(3.0)[b]	6.72(1.58)
3009.4(8.9)[c]	0.04(2)
3036.2(8.9)[c]	0.04(2)
3048.0(3.0)[b]	2.68(61)
3128.6(3.0)[b]	1.94(45)
3173.9(0.5)[d]	0.04(2)
3187.3(0.4)[b]	3.06(86)
3223.0(0.4)[b]	9.48(3.47)
3285.7(0.5)[d]	0.05(3)
3299.1(0.5)[d]	0.02(1)
3308.0(0.5)[d]	0.06(3)
3338.4(0.5)[d]	0.25(8)
3378.7(0.4)[b]	3.28(75)
3402.8(0.5)[d]	1.3(5)
3458.3(0.5)[d]	1.5(5)
3476.2(0.4)[b]	0.74(17)
3517.3(0.5)[d]	1.3(4)
3560.3(0.5)[d]	2.1(7)
3595.2(0.5)[d]	1.7(6)
3649.2(4.0)[b]	1.85(51)
3725.1(8.9)[e]	6.8(2.3)
3804.3(4.0)[b]	4.32(1.34)
3824.5(4.0)[b]	5.98(1.80)
3836.9(8.9)[e]	4.1(1.4)
3859.2(8.9)[e]	7.3(2.5)
3912.9(8.9)[e]	2.1(7)
3966.6(8.9)[e]	6.8(2.3)
4041.7(8.9)[e]	1.6(6)
4061.4(8.9)[e]	5.8(2.0)
4107.0(8.9)[e]	16.0(5.0)
4144.6(8.9)[e]	2.0(1.2)
4166.1(8.9)[e]	1.1(5)
4191.1(8.9)[e]	5.0(1.7)
4223.3(8.9)[e]	10.0(3.0)
4234.1(8.9)[e]	10.0(3.0)

[a] Resonance strength and energy adopted from the present work.

[b] Resonance strength and energy adopted from the weighted average of literature values.

[c] Resonance strength and energy adopted from Ref. [9].

[d] Resonance strength and energy adopted from Ref. [14].

[e] Resonance strength and energy adopted from Ref. [13].

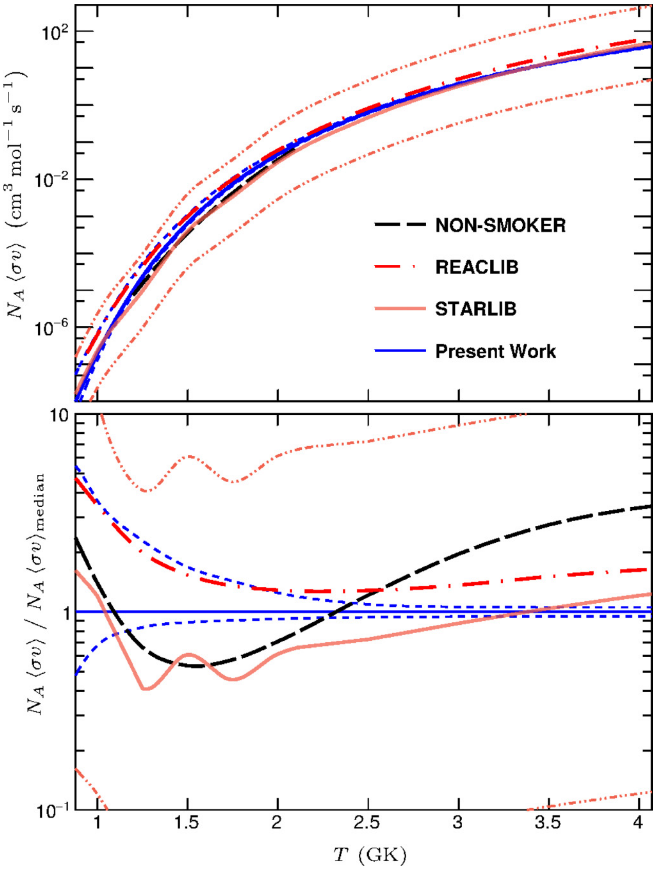

FIG. 10. Top panel: Median total thermonuclear reaction rate and associated $1-\sigma$ quantiles (blue dashed lines) calculated using the values in Table IV as input for the STARLIB rate calculator [38]. Bottom panel: NON-SMOKER [40], REACLIB [41], and STARLIB [38] rates normalized to the median total rate calculated in the present work. The STARLIB rate is calculated from the TALYS [42,43] code and is plotted with its recommended factor uncertainty (orange dash-double-dotted lines). See text for details.

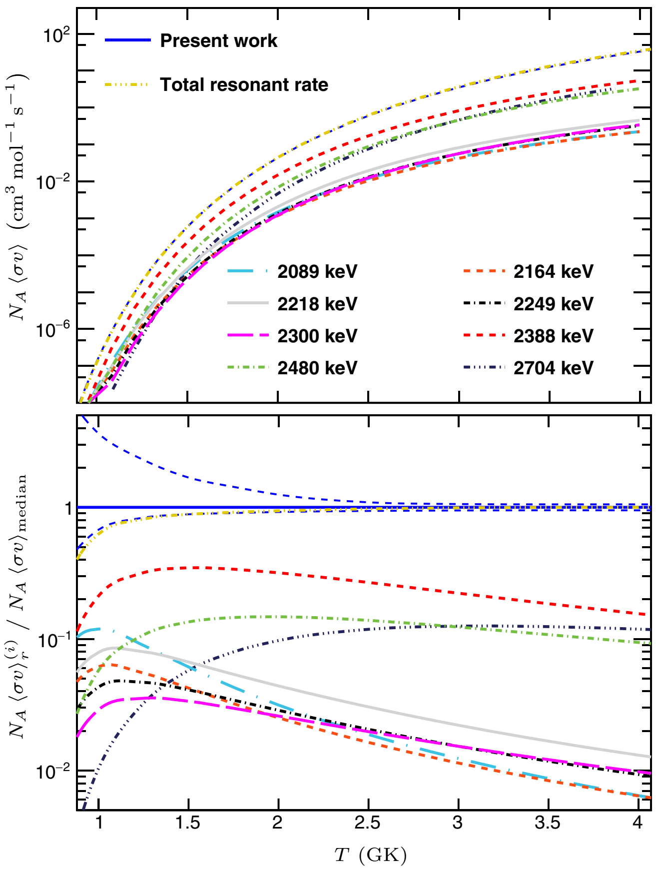

FIG. 11. Top panel: Resonant reaction rates calculated from the results of the present work compared to the median total rate calculated in the present work and the total resonant reaction rate calculated from Eq. 8 using the values in Table IV. Bottom panel: Resonant rates normalized to the median total rate calculated in the present work.

their respective uncertainties) were calculated in the usual way:

$$\overline{\mu} = \frac{\sum_i \mu_i/\sigma_i}{\sum_i 1/\sigma_i}, \quad \overline{\sigma} = \sqrt{\frac{1}{\sum_i 1/\sigma_i}}, \tag{7}$$

where μ_i is the reported measurement value (resonance energy or strength) and σ_i is the measurement's requisite uncertainty. The resonance energies and strengths used in the STARLIB rate calculation are listed in Table IV and the resulting median rate and its requisite $1-\sigma$ quantiles are compared in Fig. 10 with the NON-SMOKER [40] model as well as the recommended REACLIB [41] and the existing STARLIB [38] library rates over the temperature range relevant to explosive and nonexplosive oxygen burning ($T = 3$–4 GK and $T = 1.5$–2.7 GK, respectively). The existing STARLIB library rate is calculated from the TALYS [42,43] code [38], and has a factor uncertainty of 10 over the relevant temperature range (i.e., the "high" and "low" rates associated with the $1-\sigma$ quantiles of the rate pdf are ± 10 times the median rate). The nonresonant contribution to the reaction rate was included in the STARLIB rate calculation by adopting the value of $S(0) = 3.38 \times 10^{15}$ keV b for the astrophysical S factor at zero energy (with $S'(0) = S''(0) = 0$), an uncertainty factor of 10 and a cutoff energy of 2098 keV based on the Scott *et al.* [3] parametrization of the ^{34}S$(\alpha,\gamma)^{38}$Ar reaction rate below $T = 1$ GK (see Table 2 and Eq. (1) in Ref. [3] as well as Ref. [44]). It should be noted that the inclusion or exclusion of the nonresonant contribution from the STARLIB calculation has a minimal effect on the median rate over the temperature range of interest. This is illustrated in figure Fig. 11, where the total resonant rate is compared to the STARLIB median rate, as well as the contributions from the narrow resonances measured in the present work. From the bottom panel of Fig. 11 it is evident that the total resonant rate differs from the median rate by at most 10% in the temperature range of $T = 1$–4 GK. The total resonant rate was calculated from the resonance energies and strengths in Table IV using the familiar equation [45]

$$N_A\langle\sigma v\rangle_r = \frac{1.5394 \times 10^{11}}{(\mu T_9)^{3/2}} \sum_i (\omega\gamma)_i e^{-11.605 E_{r_i}/T_9}, \tag{8}$$

where $N_{\mathrm{A}}\langle\sigma v\rangle_r$ is the resonant reaction rate in units of cm^3 mol^{-1} s^{-1}, $\mu = 3.581$ is the reduced mass of the ^{34}S + α

system, T_9 is the temperature in units of GK, and $(\omega\gamma)_i$ and E_{r_i} are (respectively) the resonance strength and energy of the ith resonance and are expressed in units of MeV.

The individual contributions from the resonances measured in this work are compared to the median total rate in Fig. 11. From Eq. 8, one might reasonably expect low energy resonances to dominate the thermonuclear reaction rate. However, sufficiently weak resonances may not contribute significantly to the thermonuclear reaction rate owing to the linear dependence of Eq. 8 on the resonance strength. This is the case for the resonances below $E_{\mathrm{CM}} = 2388$ keV studied in the present work. Although these resonances are lower in energy than any previous resonance measurements, their strengths are sufficiently weak that their contribution is small at oxygen-burning and explosive oxygen-burning temperatures. This is illustrated in Fig. 11, from which it is clear that the contribution from the $E_{\mathrm{CM}} = 2388$ keV resonance dominates the reaction rate at oxygen-burning temperatures, while the $E_{\mathrm{CM}} = 2480$ keV resonance contributes about a factor of 2 lower and the contributions from the resonances below 2388 keV are lower by at least a factor of 4. At explosive oxygen-burning temperatures ($T = 3$–4 GK), the $E_{\mathrm{CM}} = 2704$ keV, $E_{\mathrm{CM}} = 2480$ keV, and $E_{\mathrm{CM}} = 2388$ keV resonances contribute roughly equally to the total resonant rate, while the contributions from the resonances below 2388 keV are at least a factor of 10 lower. As can be seen, for the case of the $^{34}\mathrm{S}(\alpha,\gamma)^{38}\mathrm{Ar}$ reaction, the statistical models describe the total thermonuclear reaction rate well over explosive and nonexplosive oxygen-burning temperature ranges. The median rate and requisite $1-\sigma$ quantiles calculated in this work establish a statistically meaningful $^{34}\mathrm{S}(\alpha,\gamma)^{38}\mathrm{Ar}$ thermonuclear reaction rate uncertainty and significantly reduces the uncertainty associated with the existing STARLIB library rate over explosive and nonexplosive oxygen-burning temperatures ($T = 3$–4 GK and $T = 1.5$–2.7 GK, respectively).

VI. CONCLUSIONS

A direct measurement of narrow resonances in $^{34}\mathrm{S}(\alpha,\gamma)^{38}\mathrm{Ar}$ lying within the energy range relevant to hot and explosive astrophysical environments ($E_{\mathrm{CM}} = 1.94$–3.42 MeV at $T = 2.2$ GK) was performed with the DRAGON recoil mass separator. The strengths and energies of eight resonances were measured. Of the eight resonance strengths measured, five had not been previously studied. However, it was determined that the additional lower energy resonances do not contribute significantly to the total thermonuclear reaction rate. A median total rate calculated using data from the present work (along with existing literature values) and the STARLIB rate calculator agrees with the NON-SMOKER Hauser-Feshbach statistical model calculation as well as the REACLIB and STARLIB library rates over the temperature ranges relevant for explosive and nonexplosive oxygen burning ($T = 3$–4 GK and $T = 1.5$–2.7 GK, respectively). The $1-\sigma$ quantiles of the median rate quantify a statistically meaningful rate uncertainty and are a significant reduction of the recommended uncertainty associated with the existing STARLIB rate.

ACKNOWLEDGMENTS

The authors would like to thank the beam delivery and ISAC operations groups at TRIUMF. We would also like to specifically acknowledge K. Jayamanna for his expertise and tireless work in beam production and P. Machule for his diligent maintenance of DRAGON. The authors gratefully acknowledge funding from the United States Department of Energy Office of Nuclear Physics via Grant No. DE-FG02-93ER40789, as well as the Natural Sciences and Engineering Research Council of Canada (NSERC). Authors from the UK gratefully acknowledge funding from the Science and Technology Facilities Council.

[1] C. Iliadis, *Nuclear Physics of Stars* (Wiley-VCH, Berlin, 2008), pp. 311–337,412–420.
[2] S. E. Woosley, W. D. Arnett, and D. D. Clayton, Astrophys. J. Suppl. S. **26**, 231 (1973).
[3] A. F. Scott, A. J. Morton, S. G. Tims, V. Y. Hansper, and D. G. Sargood, Nucl. Phys. A **552**, 363 (1993).
[4] D. Arnett, *Supernovae and Nucleosynthesis: An Investigation of the History of Matter from the Big Bang to the Present* (Princeton University Press, Princeton, NJ, 1996), pp. 260–267.
[5] E. Bravo and G. Martínez-Pinedo, Phys. Rev. C **85**, 055805 (2012).
[6] P. M. Endt, Nucl. Phys. A **521**, 1 (1990).
[7] T. Rauscher, Phys. Rev. C **81**, 045807 (2010).
[8] A. Chieffi, M. Limongi, and O. Straniero, Astrophys. J. **502**, 737 (1998).
[9] K. N. Sinha, A. G. Hwang, H. B. Mak, and H. C. Evans, Can. J. Phys. **57**, 781 (1979).
[10] F. C. Erne and C. Van Der Leun, Nucl. Phys. **52**, 515 (1964).
[11] R. E. Clarke, F. E. Dunnam, and H. A. Van Rinsvelt, Nucl. Phys. A **171**, 298 (1971).
[12] C. Badenes, K. J. Borkowski, and E. Bravo, Astrophys. J. **624**, 198 (2005).
[13] A. Chevallier, E. Bozek, J. Chevallier, A. Pape, and R. Armbruster, Nucl. Phys. A **191**, 201 (1972).
[14] Z. Fülöp, G. Lévai, E. Somorjai, À. Kiss, J. Cseh, P. Tikkanen, and J. Keinonen, Nucl. Phys. A **604**, 286 (1996).
[15] F. Glatz, G. Pappert, and A. Brachat, Z. Phys. A: Atoms Nuclei **278**, 319 (1976).
[16] J. A. Cameron and B. Singh, Nucl. Data Sheets **109**, 1 (2008).
[17] J. F. Ziegler, M. D. Ziegler, and J. P. Biersack, Nucl. Instrum. Methods Phys. Res. B **268**, 1818 (2010).
[18] J. F. Ziegler, computer program SRIM-2013, http://www.srim.org/ (2013).
[19] M. Wang, G. Audi, A. H. Wapstra, F. G. Kondev, M. MacCormick, X. Xu, and B. Pfeiffer, Chin. Phys. C **36**, 1603 (2012).
[20] W. R. Phillips, Nucl. Phys. **60**, 544 (1964).
[21] E. R. Flynn, O. Hansen, R. F. Casten, J. D. Garrett, and F. Ajzenberg-Selove, Nucl. Phys. A **246**, 117 (1975).
[22] C. W. Foltz, D. I. Sober, L. W. Fagg, H. D. Gräf, A. Richter, E. Spamer, and B. A. Brown, Phys. Rev. C **49**, 1359 (1994).
[23] T. Kern, P. Betz, E. Bitterwolf, F. Glatz, and H. Röpke, Z. Phys. A **294**, 51 (1980).

[24] K. Jayamanna, G. Wight, D. Gallop, R. Dube, V. Jovicic, C. Laforge, M. Marchetto, M. Leross, D. Louie, R. Laplante, R. Laxdal, M. McDonald, G. J. Wiebe, V. Wang, and F. Yan, Rev. Sci. Instrum. **81**, 02A331 (2010).

[25] R. E. Laxdal, Nucl. Instrum. Methods Phys. Res. B **204**, 400 (2003).

[26] D. Hutcheon, S. Bishop, L. Buchmann, M. L. Chatterjee, A. A. Chen, J. M. D'Auria, S. Engel, D. Gigliotti, U. Greife, D. Hunter *et al.*, Nucl. Instrum. Methods Phys. Res. A **498**, 190 (2003).

[27] D. G. Gigliotti, Master's thesis, University of Northern British Columbia, Prince George, Canada, 2004 (unpublished).

[28] C. Vockenhuber, L. Buchmann, J. Caggiano, A. A. Chen, J. M. D'Auria, C. Davis, U. Greife, A. Hussein, D. Hutcheon, D. Ottewell *et al.*, Nucl. Instrum. Methods Phys. Res. B **266**, 4167 (2008).

[29] G. Christian, D. A. Hutcheon, C. Akers, D. Connolly, J. Fallis, and C. Ruiz, Phys. Rev. C **88**, 038801 (2013).

[30] C. Ruiz, U. Greife, and U. Hager, Eur. Phys. J. A **50**, 99 (2014).

[31] S. Engel, Ph.D. thesis, Ruhr-Universität Bochum, Bochum, Germany, 2003 (unpublished).

[32] C. E. Rolfs and W. S. Rodney, *Cauldrons in the Cosmos Nuclear Astrophysics* (University of Chicago Press, Chicago, 1988), pp. 289–296.

[33] W. A. Rolke, A. M. López, and J. Conrad, Nucl. Instrum. Methods Phys. Res. A **551**, 493 (2005).

[34] U. Greife, S. Bishop, L. Buchmann, M. L. Chatterjee, A. A. Chen, J. M. D'Auria, S. Engel, D. Gigliotti, D. Hunter, D. A. Hutcheon *et al.*, Nucl. Instrum. Methods Phys. Res. B **217**, 1 (2004).

[35] G. Schiwietz and P. L. Grande, Nucl. Instrum. Methods Phys. Res. B **177**, 125 (2001).

[36] W. Liu, G. Imbriani, L. Buchmann, A. A. Chen, J. M. D'Auria, A. D. Onofrio, S. Engel, L. Gialanella, U. Greife, D. Hunter, and A. Hussein, Nucl. Instrum. Methods Phys. Res. B **496**, 198 (2003).

[37] D. A. Hutcheon, C. Ruiz, J. Fallis, J. M. D'Auria, B. Davids, U. Hager, L. Martin, D. F. Ottewell, S. Reeve, and A. Rojas, Nucl. Instrum. Methods Phys. Res. A **689**, 70 (2012).

[38] A. L. Sallaska, C. Iliadis, A. E. Champange, S. Goriely, S. Starrfield, and F. X. Timmes, Astrophys. J. Suppl. S. **207**, 18 (2013).

[39] R. Longland, C. Iliadis, A. Champagne, J. Newton, C. Ugalde, A. Coc, and R. Fitzgerald, Nucl. Phys. A **841**, 1 (2010).

[40] T. Rauscher and F. K. Thielemann, Atom. Data Nucl. Data **75**, 1 (2000).

[41] R. H. Cyburt, A. M. Amthor, R. Ferguson, Z. Meisel, K. Smith, S. Warren, A. Heger, R. D. Hoffman, T. Rauscher, A. Sakharuk *et al.*, Astrophys. J. Supplement Series **189**, 240 (2010).

[42] A. J. Koning, S. Hilaire, and M. Duijvestijn, TALYS: A nuclear reaction program, NRG Report 2129704.62741P, Petten, Netherlands, 2004 (unpublished).

[43] S. Goriely, S. Hilaire, and A. J. Koning, Astron. Astrophys. **487**, 767 (2008).

[44] S. Woosley, W. A. Fowler, J. Holmes, and B. Zimmerman, At. Data Nucl. Data Tables **22**, 371 (1978).

[45] C. Angulo, M. Arnould, M. Rayet, P. Descouvemont, D. Baye, C. Leclercq-Willain, A. Coc, S. Barhoumi, P. Aguer, C. Rolfs *et al.*, Nucl. Phys. A **656**, 3 (1999).